Supporting Information

Contents:

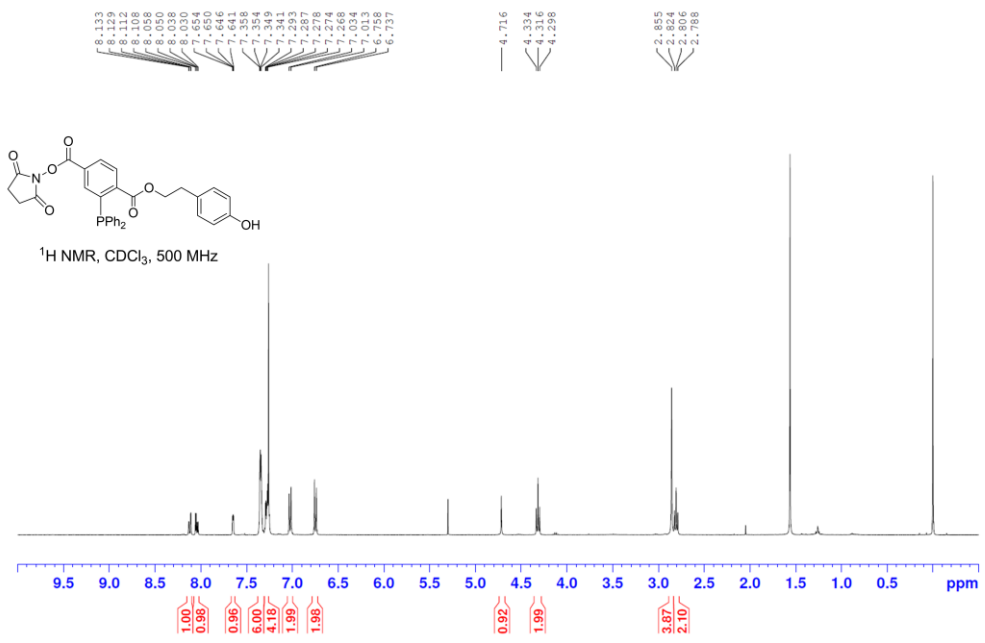

Figure S1. ^{1}H-NMR spectra for tracer DPTA (**4**).

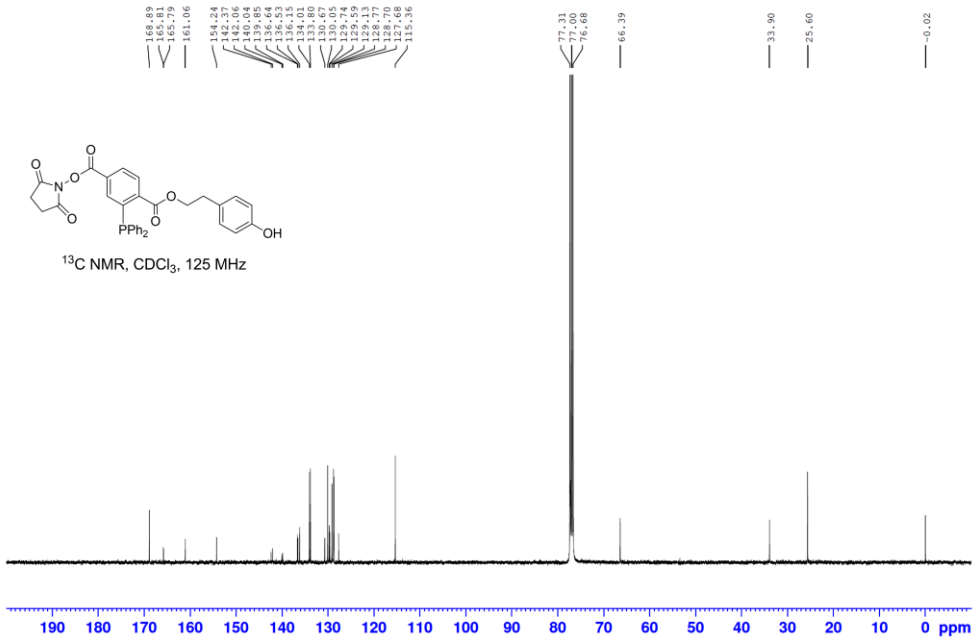

Figure S2. ^{13}C-NMR spectra for tracer DPTA (**4**).

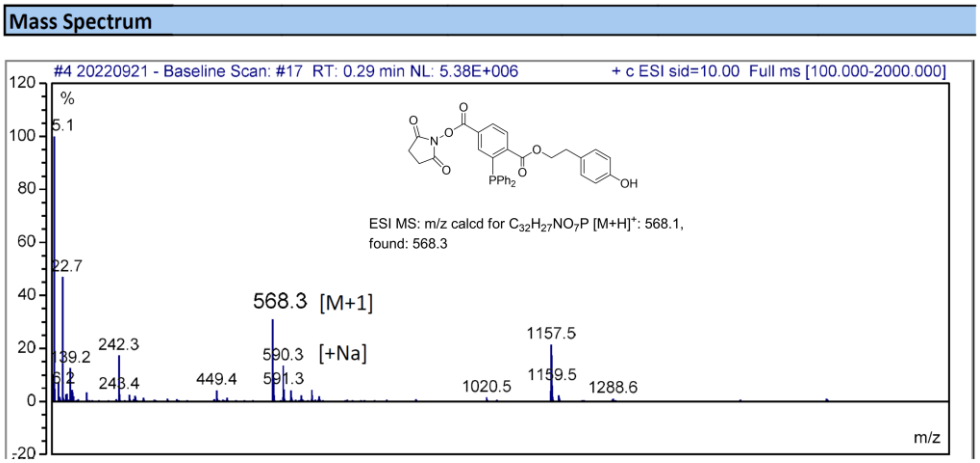

Figure S3. ESI-mass spectrometric data for tracer DPTA (**4**).

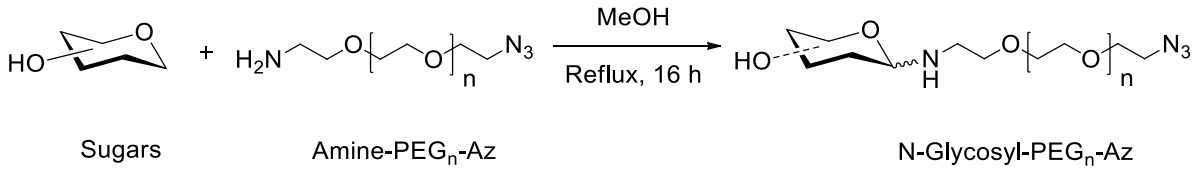

Figure S4. Schematic representation for the synthesis of N-glycosyl azides.

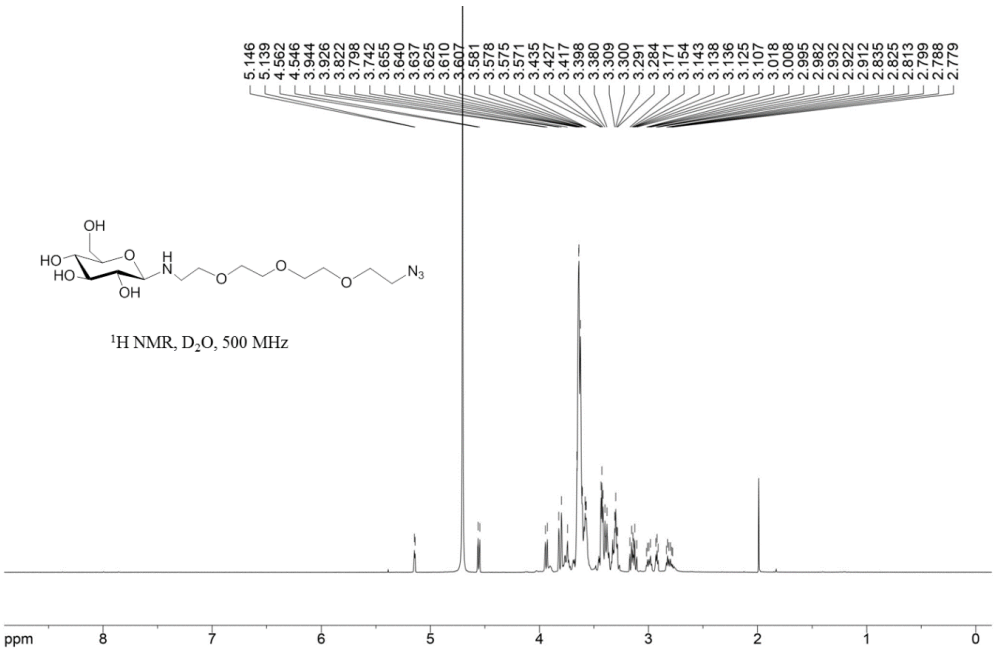

Figure S5. ^{1}H-NMR spectra for glucose-PEG$_3$-azide.

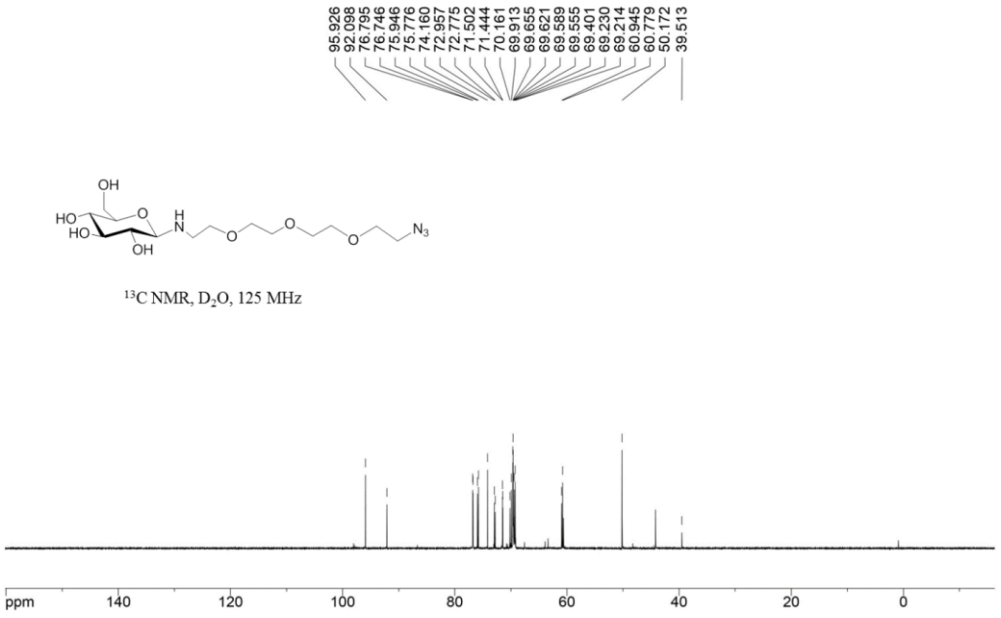

Figure S6. ^{13}C-NMR spectra for glucose-PEG$_3$-azide.

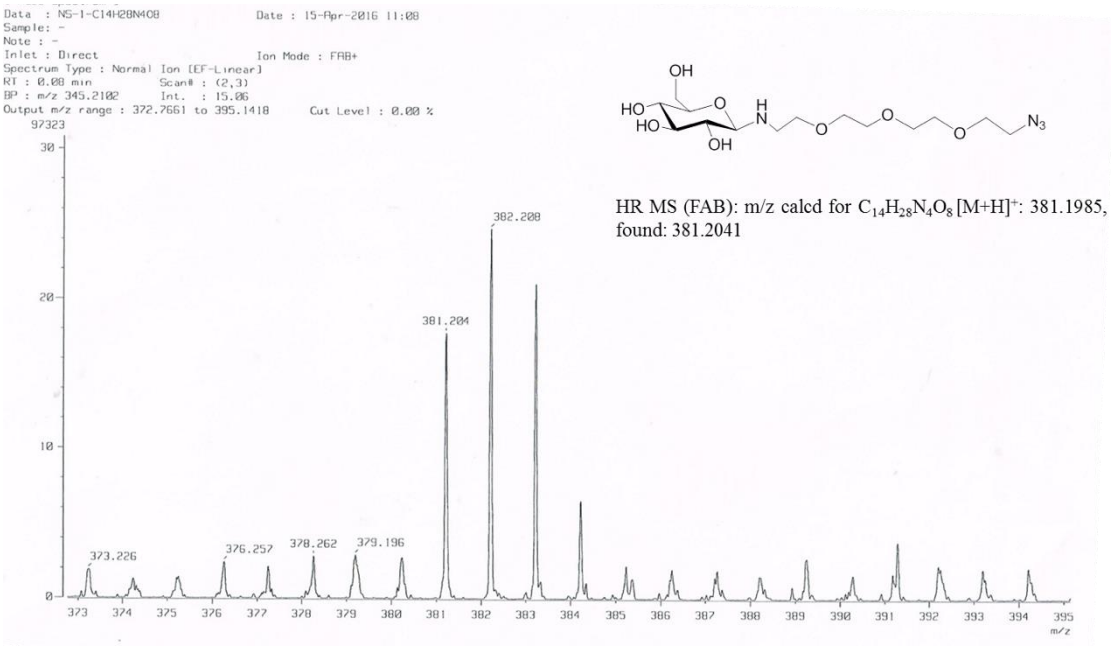

Figure S7. High resolution mass spectroscopic data for glucose-PEG$_3$-azide.

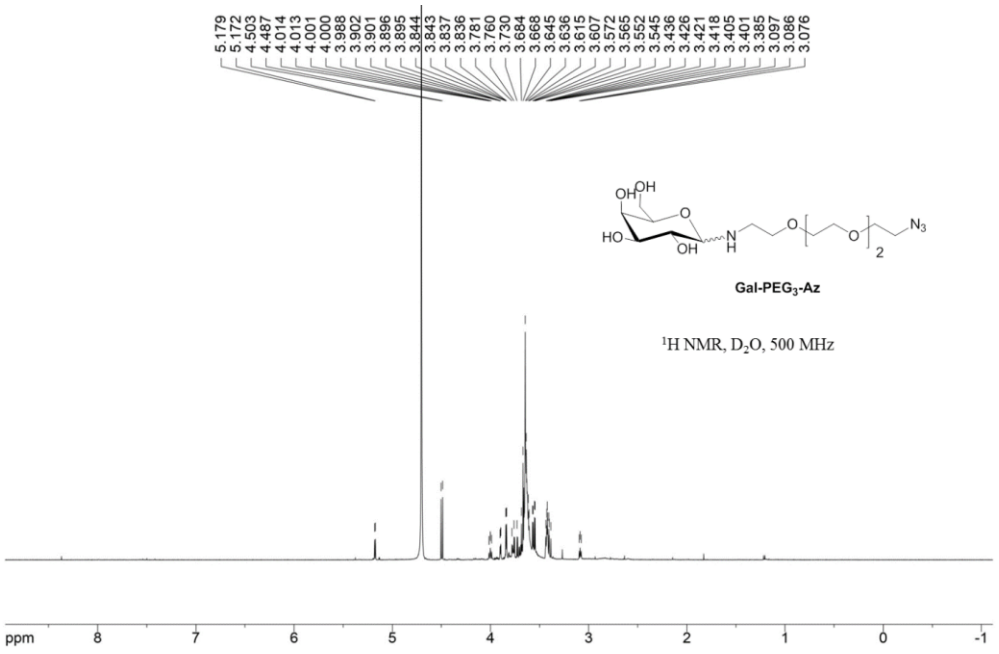

Figure S8. [1]H-NMR spectra for galactose-PEG3-azide.

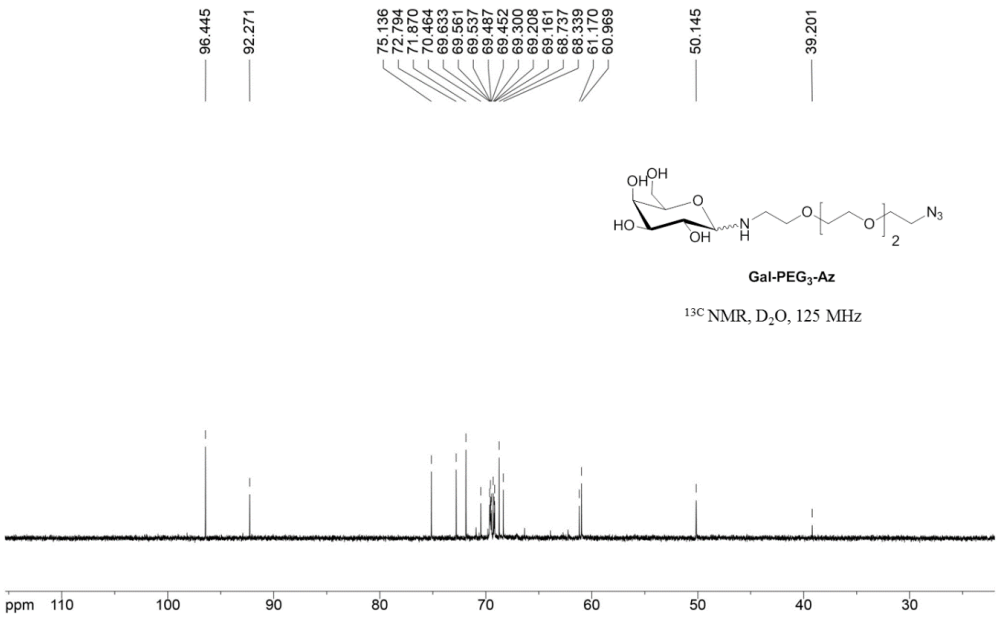

Figure S9. [13]C-NMR spectra for galactose-PEG3-azide.

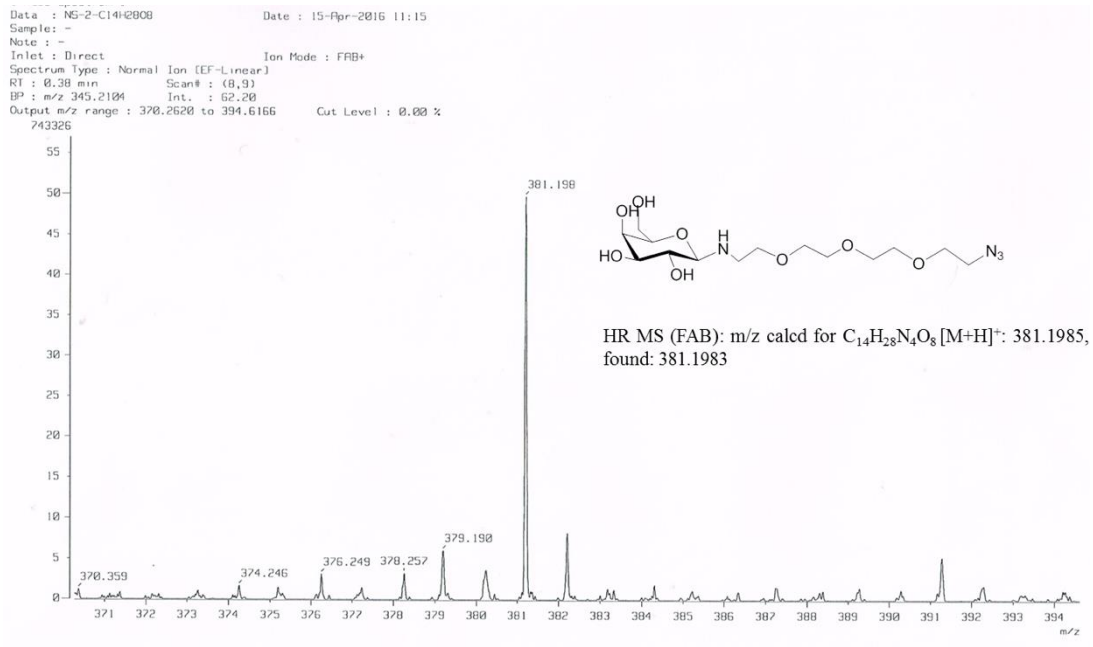

Figure S10. High resolution mass spectroscopic data for galactose-PEG3-azide.

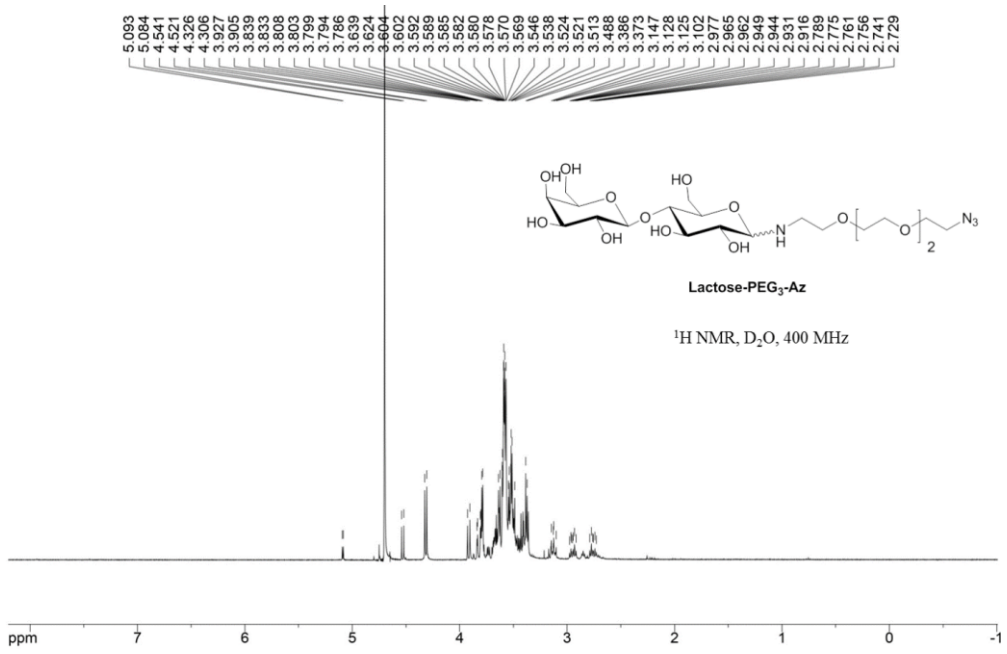

Figure S11. [1]H-NMR spectra for lactose-PEG3-azide.

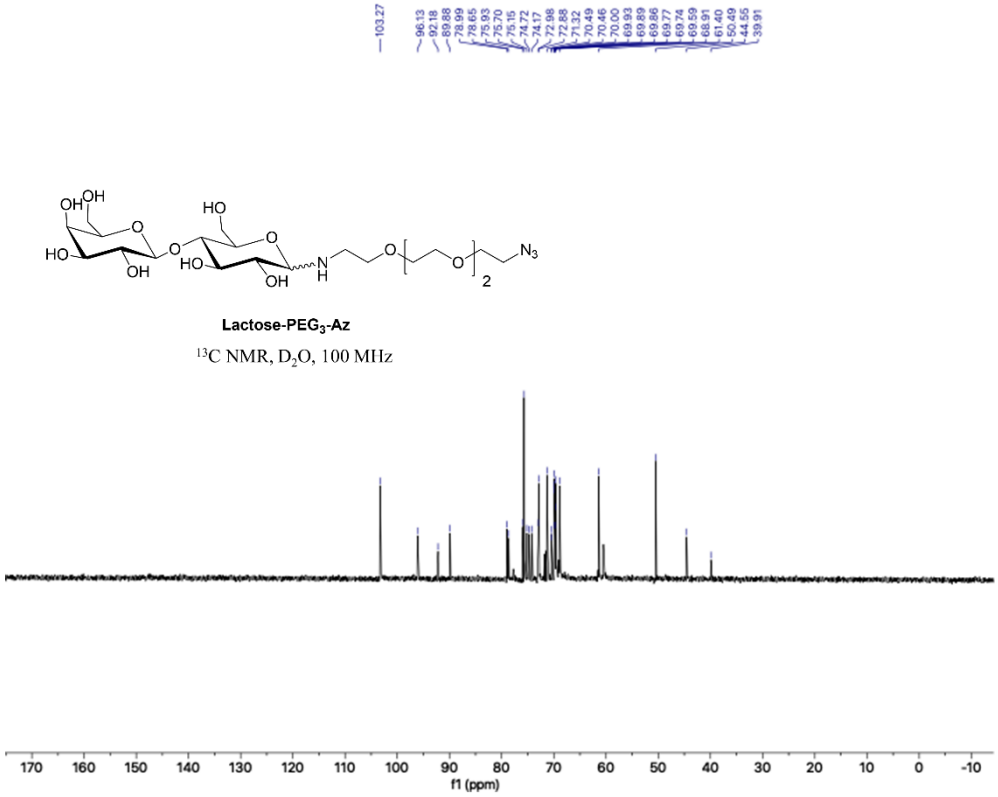

Figure S12. ^{13}C-NMR spectra for lactose-PEG$_3$-azide.

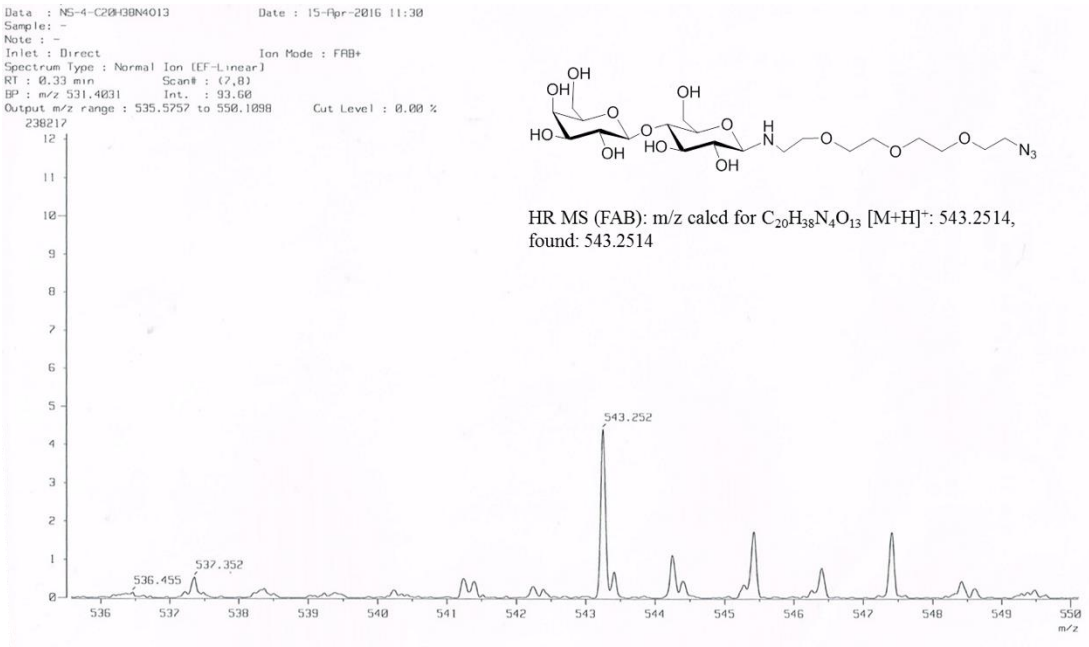

Figure S13. High resolution mass spectroscopic data for lactose-PEG$_3$-azide.

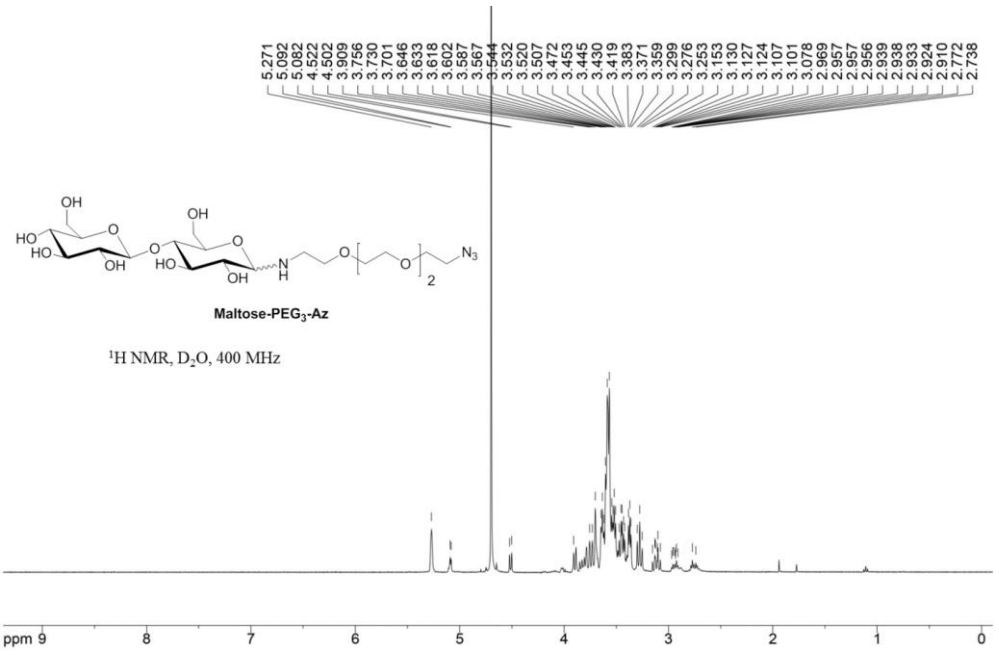

Figure S14. [1]H-NMR spectra for maltose-PEG3-azide.

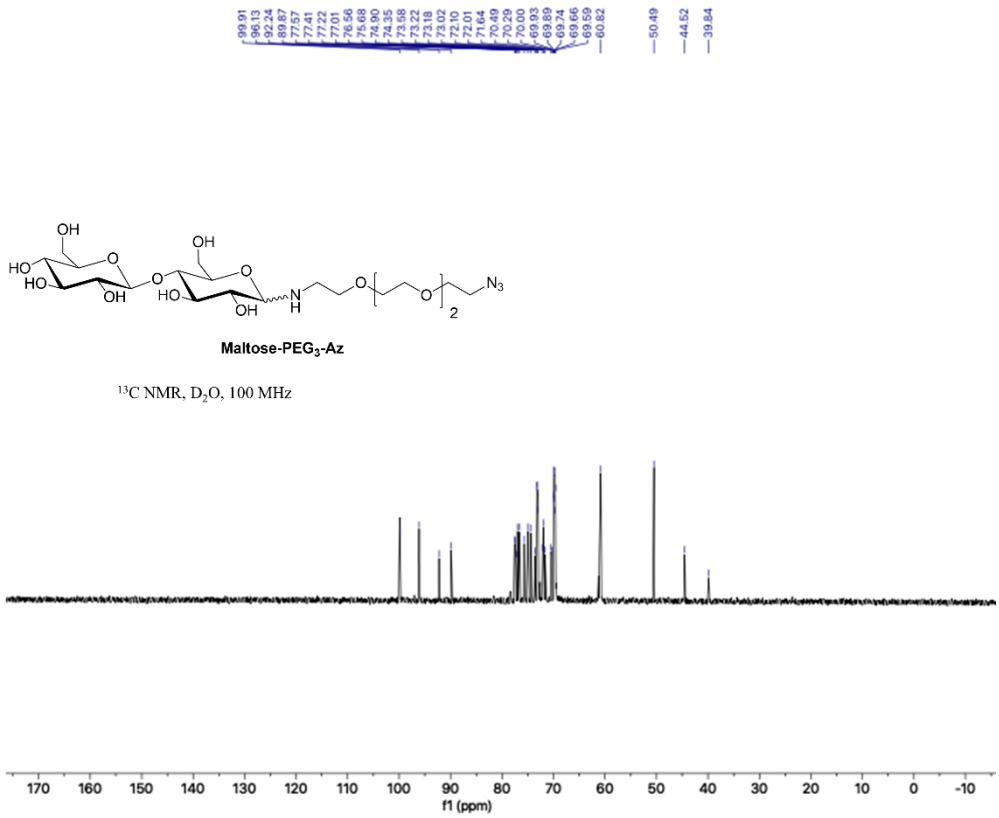

Figure S15. [13]C-NMR spectra for maltose-PEG3-azide.

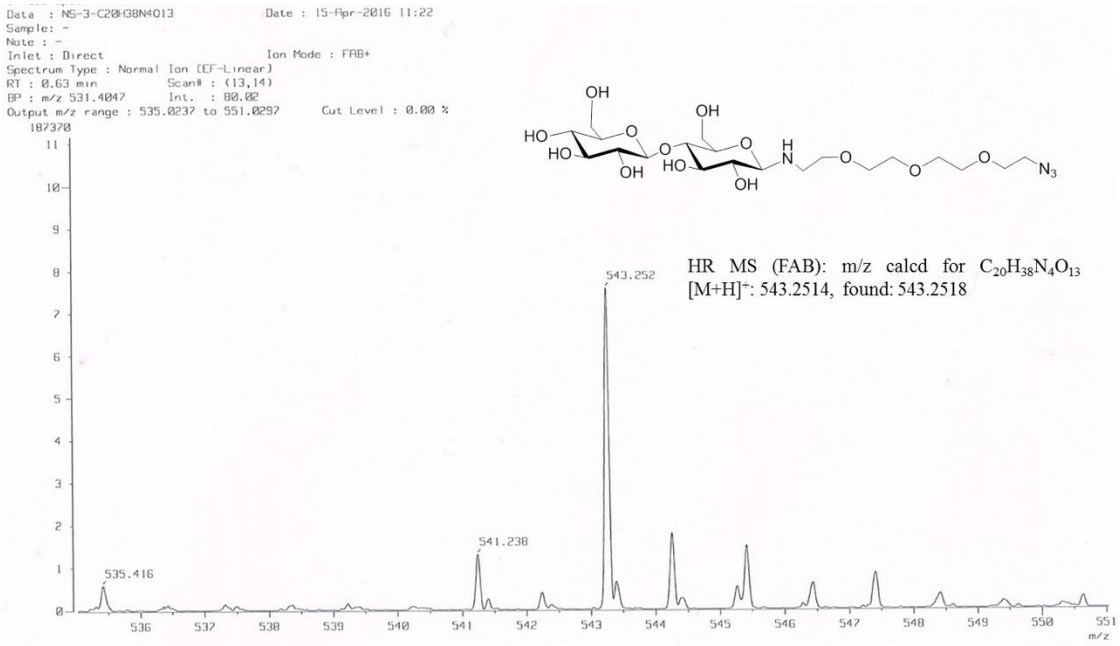

Figure S16. High resolution mass spectroscopic data for maltose-PEG3-azide.

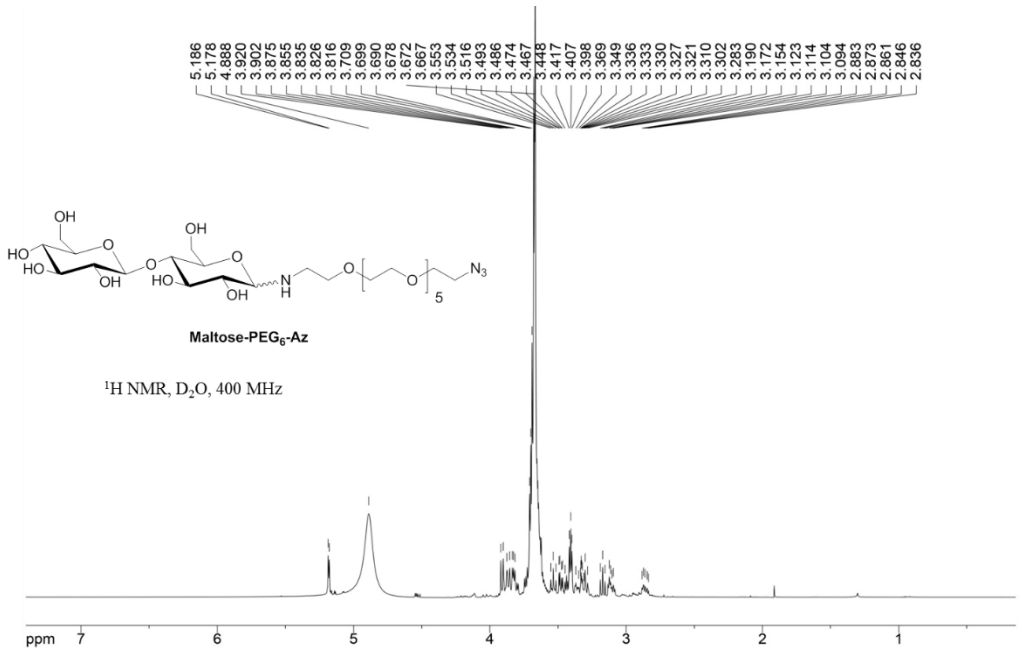

Figure S17. 1H NMR spectra for maltose-PEG6-azide.

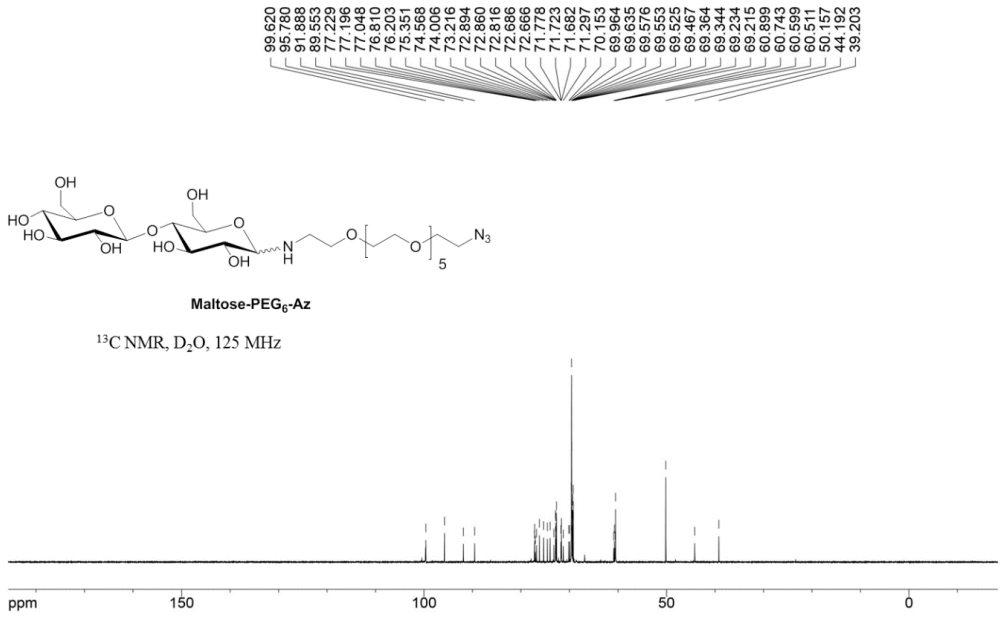

Figure S18. ^{13}C NMR spectra for maltose-PEG$_6$-azide.

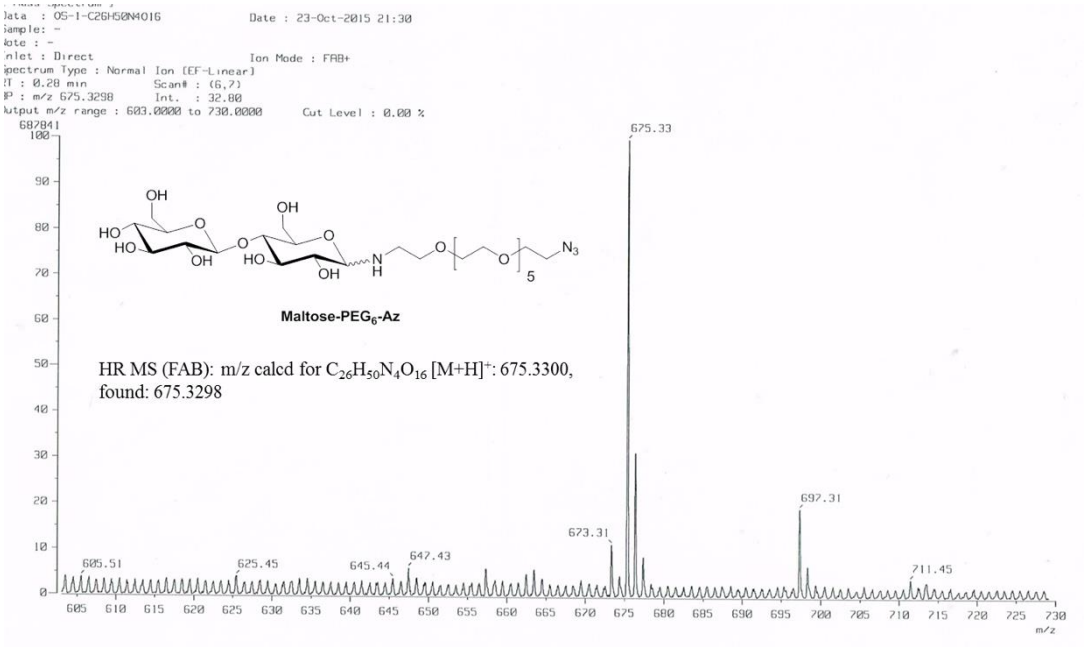

Figure S19. High resolution mass spectroscopic data for maltose-PEG$_6$-azide.

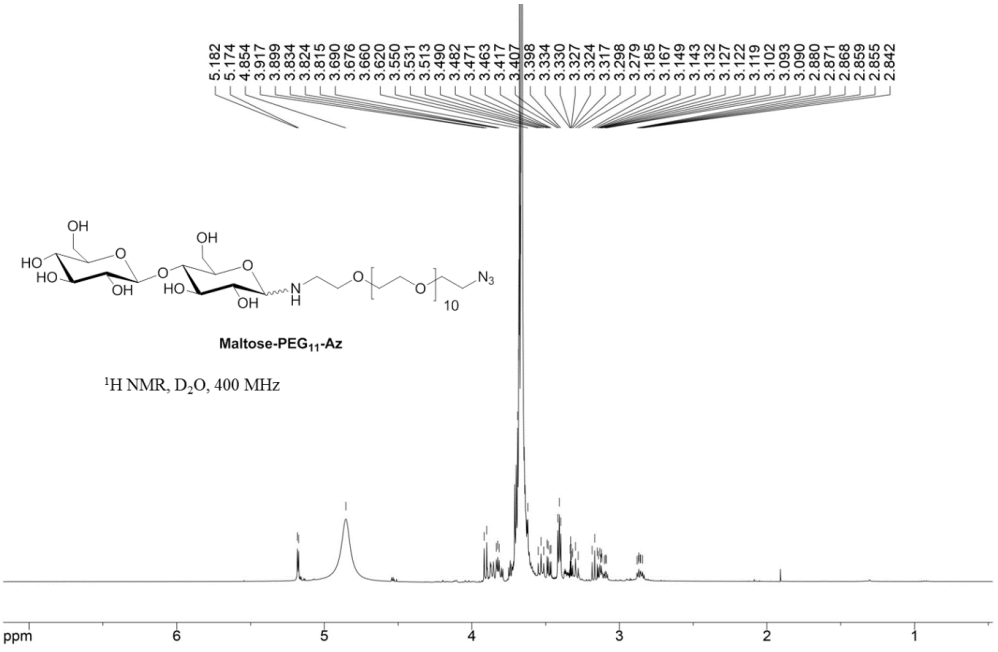

Figure S20. ^{1}H NMR spectra for maltose-PEG$_{11}$-azide.

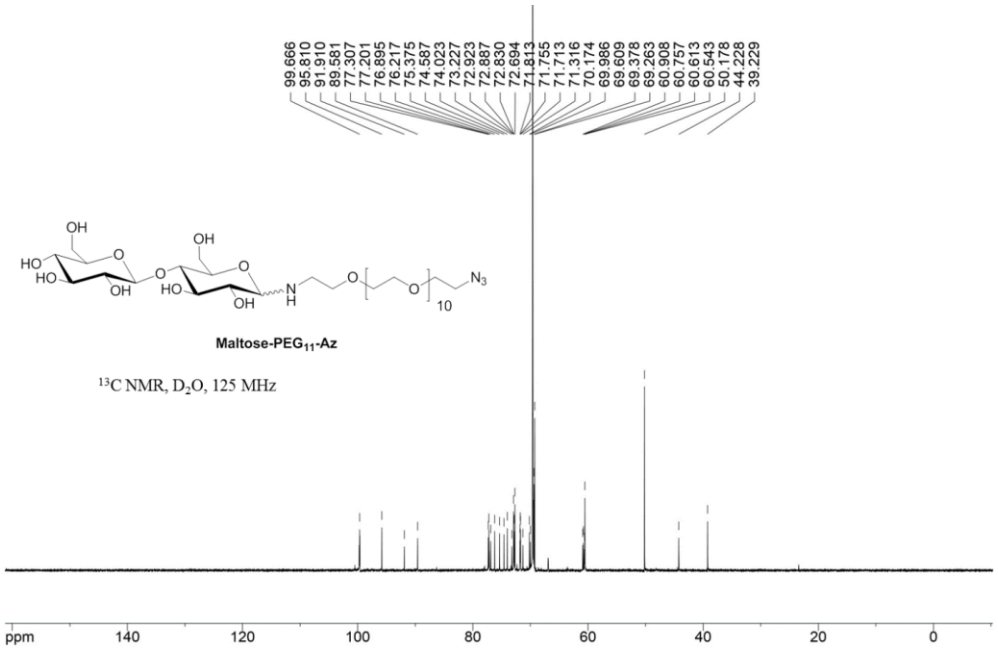

Figure S21. ^{13}C NMR spectra for maltose-PEG$_{11}$-azide.

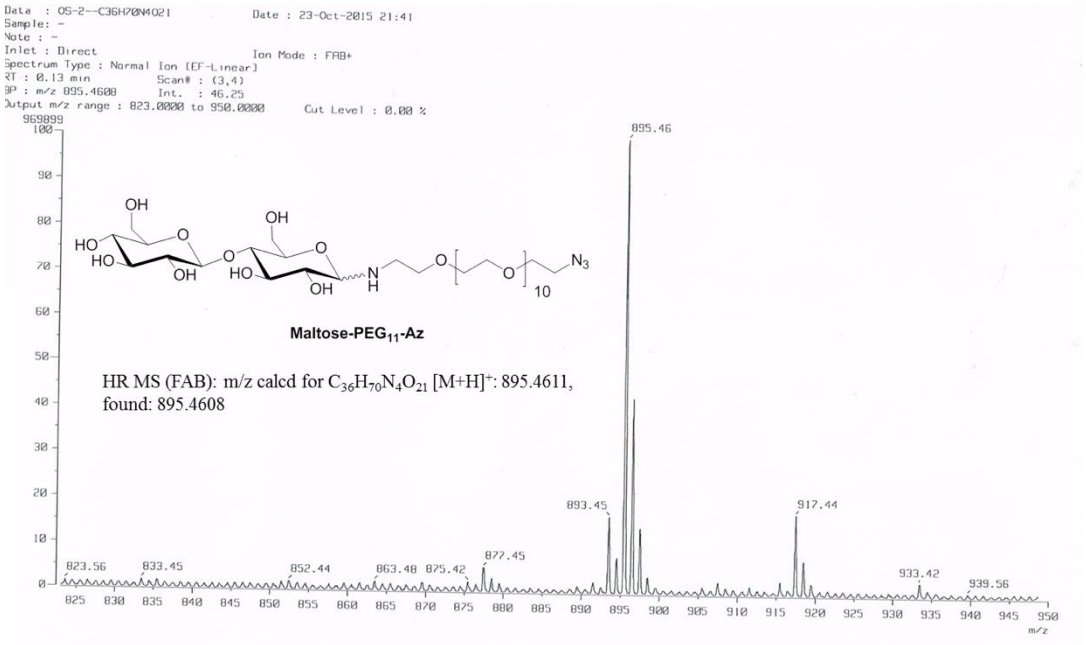

Figure S22. High resolution mass spectroscopic data for maltose-PEG11-azide.

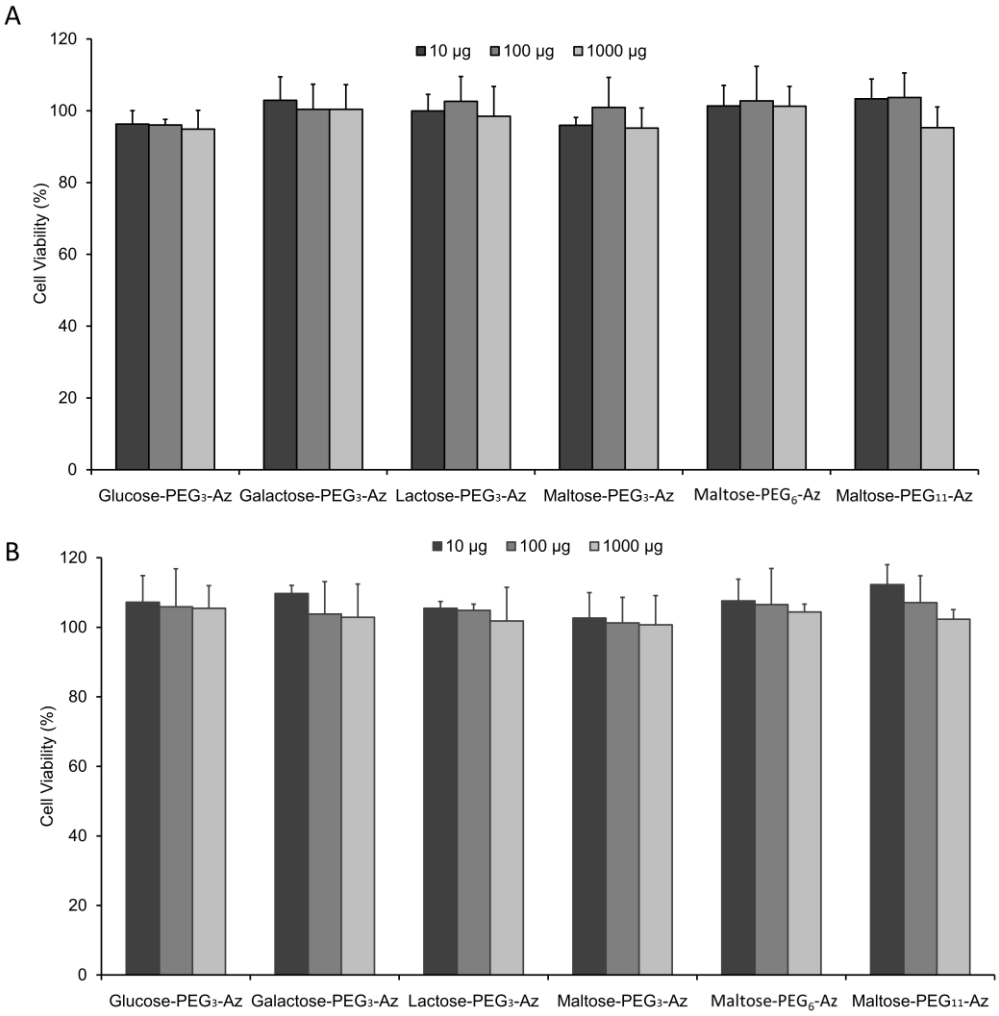

Figure S23. Cell viability of N-glycosyl azides performed in NIH3T6.7 cells by MTT assay; 7 h of treatment (**A**) and 24 h of treatment (**B**).

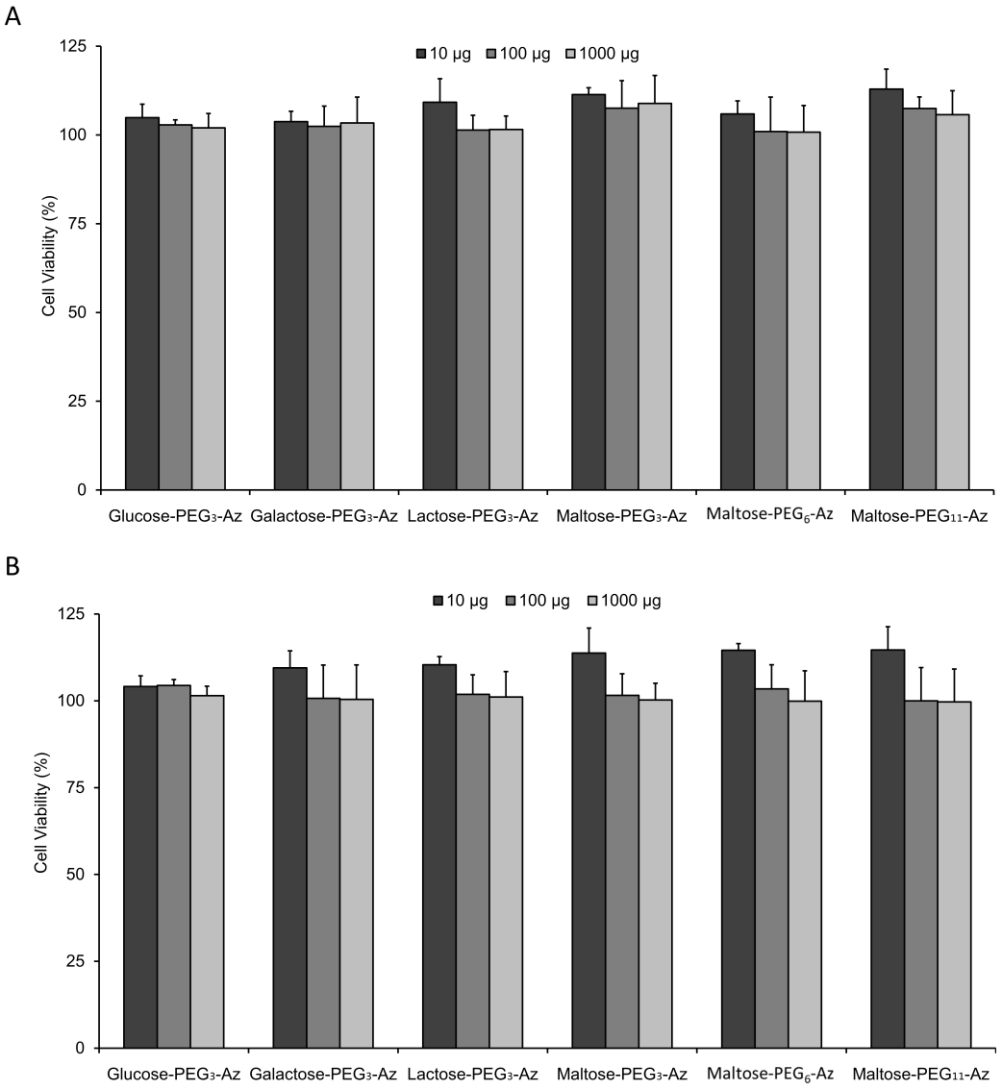

Figure S24. Cell viability of N-glycosyl azides performed in HEK293 cells by MTT assay; 7 h of treatment (**A**) and 24 h of treatment (**B**).

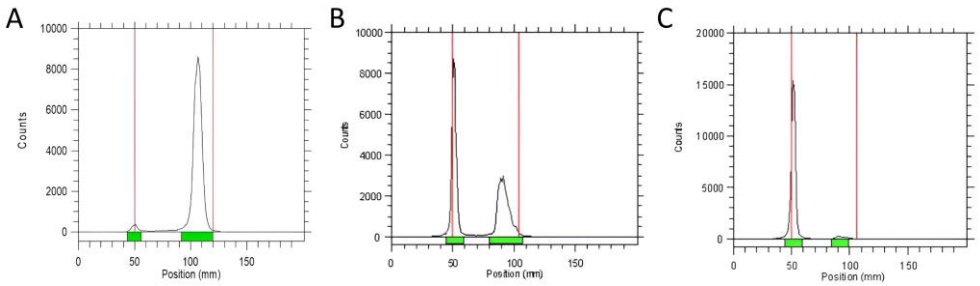

Figure S25. Representative radio thin-layer chromatograms of the radioiodinated tracer DPTA (**5**) (**A**), bioconjugation of radiotracer DPTA with trastuzumab (**B**), and the purified [^{131}I]DPTA-trastuzumab (**6**) (**C**). Radio-TLC analyses were performed on silica with methanol as mobile phase.

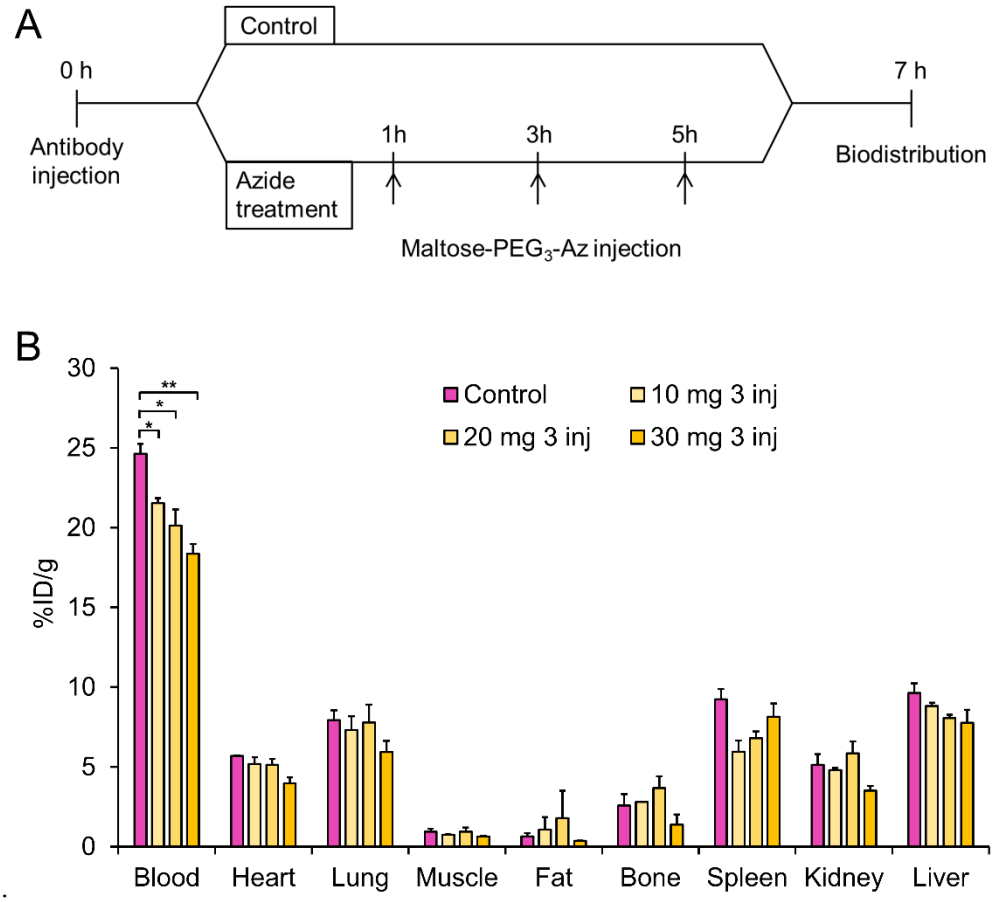

Figure S26. Schematic representation demonstrating study plan (**A**). Biodistribution data of ICR mice after injection of [^{131}I]DPTA-trastuzumab followed by varying the quantity of maltose-PEG$_3$-azide (**B**) (n = 2). *$p < 0.05$ and **$p < 0.001$.

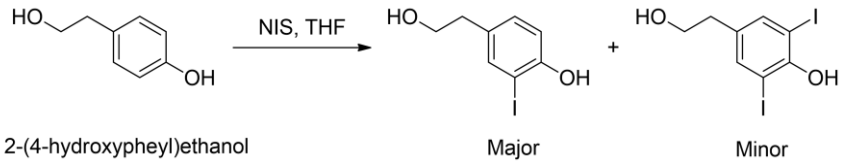

Figure S27. Synthetic scheme of non-radioactive 4-(2-hydroxyethyl)-2-iodophenol.

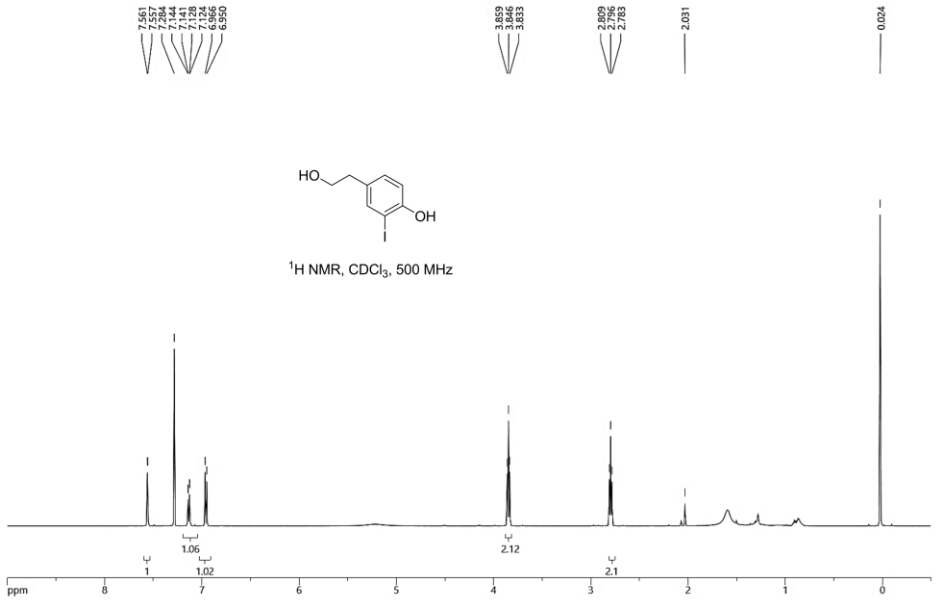

Figure S28. ^{1}H NMR spectrum of 4-(2-hydroxyethyl)-2-iodophenol.

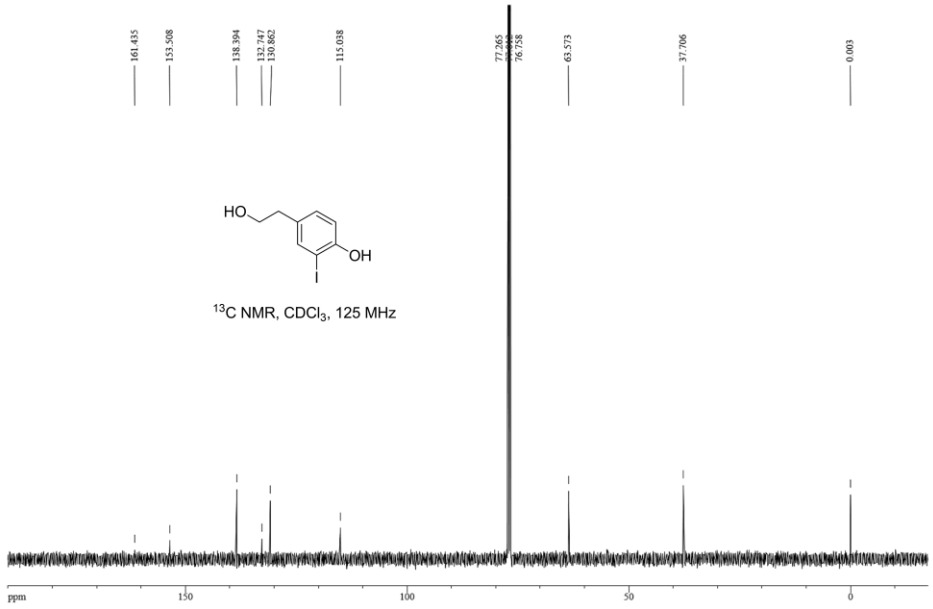

Figure S29. ^{13}C NMR spectrum of 4-(2-hydroxyethyl)-2-iodophenol.

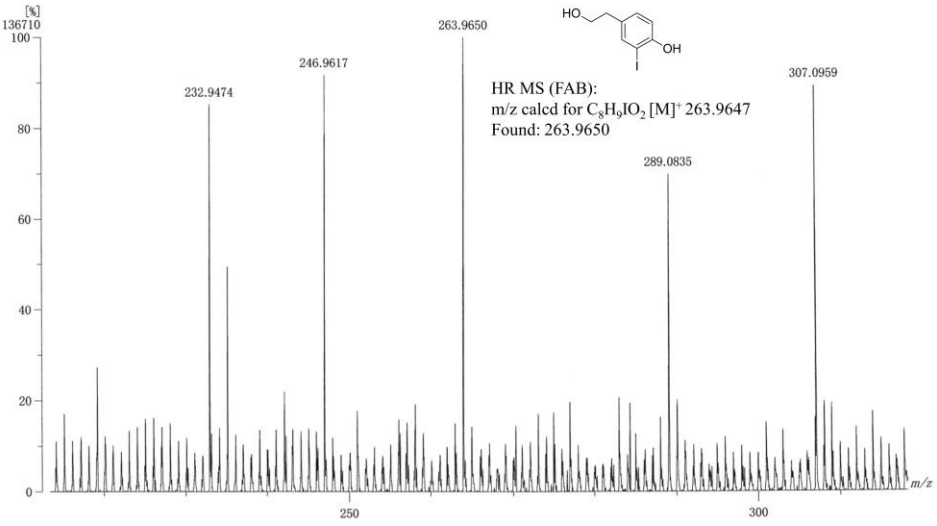

Figure S30. High resolution mass spectroscopic data for 4-(2-hydroxyethyl)-2-iodophenol.

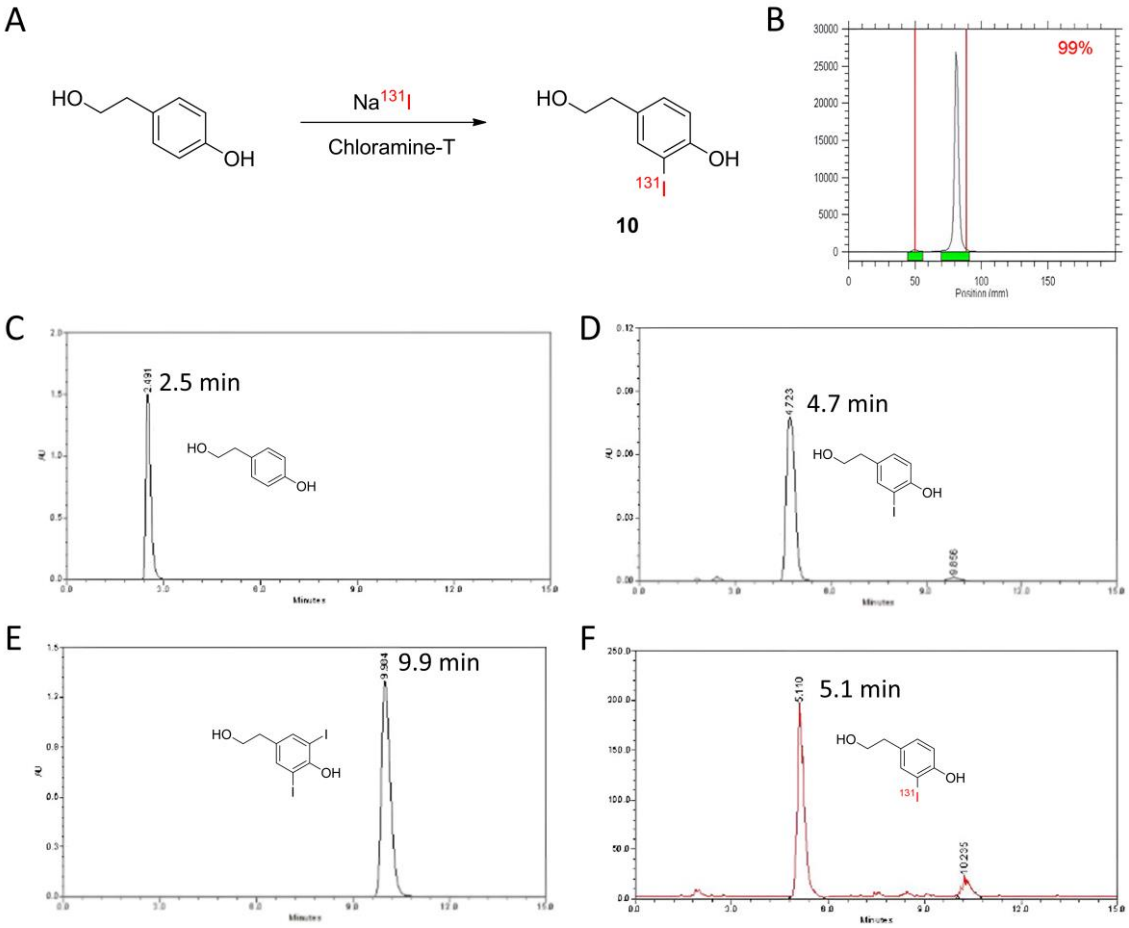

Figure S31. Schematic of radiolabeling of 4-(2-hydroxyethyl)-2-[^{131}I]iodophenol (**10**) (**A**). Radio thin-layer chromatogram of compound **10** performed in silica, ethyl acetate:methanol (95:5) (**B**). UV-HPLC chromatograms of 2-(4-hydroxyphenol) ethanol (**C**), 4-(2-hydroxyethyl)-2-iodophenol (**D**), 4-(2-hydroxyethyl)-2,6-diiodophenol (**E**) and radio-HPLC chromatogram of 4-(2-hydroxyethyl)-2-[^{131}I]iodophenol (**10**) (**F**).

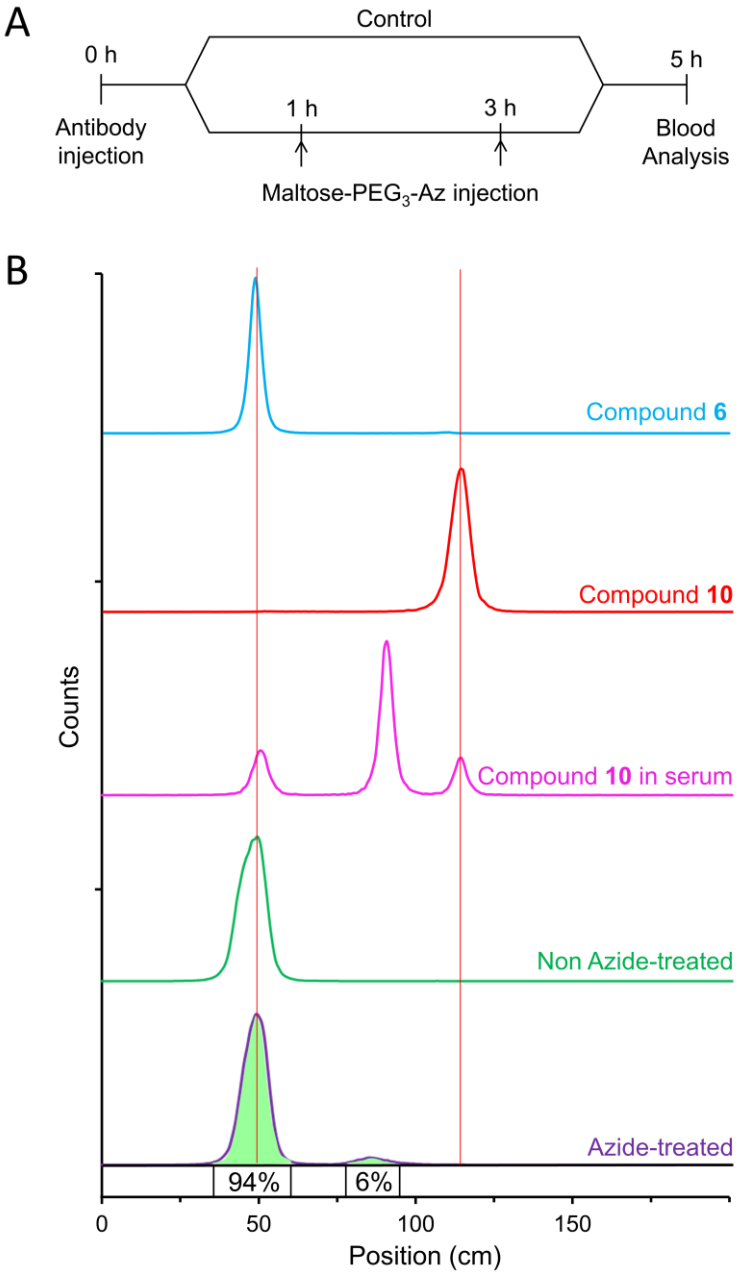

Figure S32. Radio-TLC analysis of in vivo Staudinger ligation in serum of control and azide-treated mice. Purified [^{131}I]DPTA-trastuzumab (**6**) (blue line), 4-(2-hydroxyethyl)-2-[^{131}I]iodophenol (**10**) (red line), non-azide-treated control serum (green line), maltose-PEG$_3$-azide treated serum mixed with 4-(2-hydroxyethyl)-2-[^{131}I]iodophenol (**10**) (pink line), maltose-PEG$_3$-Az treated serum (violet line). All radio-TLC were developed using iTLC and saline.

Figure S33. Biodistribution of 4-(2-hydroxyethyl)-2-[^{131}I]iodophenol (**10**) in normal ICR mice (n = 3).